NPS-EC-98-002

NAVAL POSTGRADUATE SCHOOL
Monterey, California

Algorithms for LORAN-C Time Difference Error Minimization

by

Roberto Cristi
Murali Tummala
Frederick M. France, Jr.

January 1998

Prepared for: U.S. Coast Guard
LORAN Support Unit

NAVAL POSTGRADUATE SCHOOL
Monterey, California

Rear Admiral M.J. Evans
Superintendent

R. Elster
Provost

This report was sponsored by the U.S. Coast Guard LORAN Support Unit.

Approved for public release; distribution is unlimited.

The report was prepared by:

Roberto Cristi
Associate Professor
Department of Electrical and
Computer Engineering

Murali Tummala
Professor
Department of Electrical and
Computer Engineering

Reviewed by:

HERSCHEL H. LOOMIS, JR.
Chairman
Department of Electrical and
Computer Engineering

Released by:

DAVID W. NETZER
Associate Provost and
Dean of Research

REPORT DOCUMENTATION PAGE

Form Approved
OMB No. 0704-0188

1. AGENCY USE ONLY (Leave blank)	2. REPORT DATE	3. REPORT TYPE AND DATES COVERED
	January 9, 1998	Interim Report 1 Jan-30 Sep 1997

4. TITLE AND SUBTITLE
Algorithms for LORAN-C Time Difference Error Minimization

5. FUNDING NUMBERS
DTC G23-97-XTHA122

6. AUTHOR(S)
Roberto Cristi, Murali Tummala, and Frederick M. France, Jr.

7. PERFORMING ORGANIZATION NAME(S) AND ADDRESS(ES)
Department of Electrical and Computer Engineering
Naval Postgraduate School
Monterey, CA 93943-5000

8. PERFORMING ORGANIZATION REPORT NUMBER
NPS-EC-98-002

9. SPONSORING/MONITORING AGENCY NAME(S) AND ADDRESS(ES)
U.S. Coast Guard
LORAN Support Unit
12001 Pacific Avenue
Wildwood, NJ 08260-3232

10. SPONSORING/MONITORING AGENCY REPORT NUMBER

11. SUPPLEMENTARY NOTES
The views expressed in this report are those of the author and do not reflect the official policy or position of the Department of Defense or the United States Government.

12a. DISTRIBUTION/AVAILABILITY STATEMENT
Approved for public release; distribution is unlimited.

12b. DISTRIBUTION CODE
A

13. ABSTRACT (Maximum 200 words)

The United States Coast Guard (USCG) is in the process of upgrading the hardware of the LORAN-C Radionavigation System Control System. As part of this effort, the Computer-Assisted LORAN-C Controller (CALOC), is also in need of improvement. CALOC performs four tasks: abnormality detection, time difference control, recordkeeping, and blink control. The work reported in this report focuses on time difference control. In many instances, CALOC does not accurately control the time difference error (TDE) within the established USCG control procedures. Two new algorithms are proposed here to control TDE more effectively: a proportional-integral-derivative (PID) controller and a Kalman filter. Actual TDE data recorded at three different master stations covering five LORAN-C chains is used to evaluate the performance of the proposed controllers. The PID controller shows a substantial improvement in control compared to CALOC, and the Kalman filter exhibits even better performance, based on preliminary results. This improvement in control correlates directly with an increase in both predictable accuracy and repeatable accuracy.

14. SUBJECT TERMS	15. NUMBER OF PAGES
LORAN-C, PID Controller, Kalman filter, time difference error	25
	16. PRICE CODE

17. SECURITY CLASSIFICATION OF REPORT	18. SECURITY CLASSIFICATION OF THIS PAGE	19. SECURITY CLASSIFICATION OF ABSTRACT	20. LIMITATION OF ABSTRACT
UNCLASSIFIED	UNCLASSIFIED	UNCLASSIFIED	SAR

Abstract

The United States Coast Guard (USCG) is in the process of upgrading the hardware of the Loran-C Radionavigation System Control System. As part of this effort, the Computer-Assisted Loran-C Controller (CALOC), is also in need of improvement. CALOC performs four tasks: abnormality detection, time difference control, recordkeeping, and blink control. The work reported in this report focuses on time difference control. In many instances, CALOC does not accurately control the time difference error (TDE) within the established USCG control procedures. Two new algorithms are proposed here to control TDE more effectively: a proportional-integral-derivative (PID) controller and a Kalman filter. Actual TDE data recorded at three different master stations covering five Loran-C chains is used to evaluate the performance of the proposed controllers. The PID controller shows a substantial improvement in control compared to CALOC, and the Kalman filter exhibits even better performance, based on preliminary results. This improvement in control correlates directly with an increase in both predictable accuracy and repeatable accuracy.

1 Introduction

The problem of designing a system which automatically corrects for phase drifts in a LORAN-C application has been addressed in this research.

As described in [1] plans exist to upgrade the existing hardware of LORAN-C stations, and implement the system on Unix workstations. However the existing software, based on the CALOC implementation, needs to be redesigned to take advantage of more modern techniques in estimation and control which can be implemented in realtime with currently available hardware.

In this report we propose two algorithms to compute the Local Phase Adjustment (LPA) corrections. One is based on standard PID control (Proportional, Integral, Derivative) and the other is based on a combination of a Kalman filter and an Optimal controller.

The two algorithms have been tested on a limited set of data, and there is a strong indication that their performance represents an improvement with respect to the CALOC algorithm as currently implemented. The improvements seem to be twofold: a) both the Time Difference Error (TDE) and the cumulative TDE are lower than in the current implementation, and b) the number of corrections is not increased with respect to what is currently available.

The advantage of the second approach, which we call *Model Based*, is that a model of the disturbances is part of the formulation. In this way further improvements can be expected by modeling the errors involved, due to short time fluctuations, periodic (daily) perturbations and long term effects. A tuning algorithm, which could be adaptive, operator driven or a combination of both, can be designed to take maximum advantage of all apriori knowledge we have of the disturbances. In particular daily and seasonal periodicities can be exploited to reduce the TDE.

This report is organized as follows. Section 2 presents the results on the PID control implementation, while the optimal control/estimator approach is shown in section 3. Recommendations for further research are given in the final section.

2 Proportional-Integral-Derivative Control Algorithm

In this section, an algorithm based on the proportional-integral-derivative (PID) controller is developed. The input is actual data from operational Loran-C chains and the output values are local phase adjustments (LPAs). These LPAs are used to help maintain the station pulse transmission timing in line with the USCG established control procedures. The data provided is preprocessed in order to remove the influence of the current controller, CALOC, to obtain uncontrolled data. The data is filtered to remove the high frequency noise components and then passed through the PID controller. The output of the controller is quantized to produce LPAs in quanta of 20 ns for pulse timing correction. The results of this controller show improved control of both the current time difference error (TDE) and the cumulative TDE over the existing control algorithm.

2.1 Time Difference Error (TDE) Data Sets

The data sets used in this research were collected during three distinct times of the year. The data from Malone, Florida, was collected during the winter; data from Middletown, California, was collected during the late spring; and the data from Kodiak, Alaska, was collected during the fall. This gave some indication of seasonal weather effects, however, no conclusions could be drawn from the limited data sets and the fact that each chain's data set included at most two days' worth of data.

2.1.1 Limitations

There were several limitations in the data sets used in this work. The most significant of these was that the data sets did not contain 24 hours worth of data points. The initial data sets from Malone, Florida were missing anywhere from 65 minutes to as much as 164 minutes of data points. This precluded an exact correlation with the CALOC-generated strip charts and forced a different approach for comparison. After isolating and correcting the cause of the missing data points, the data sets from Middletown, California, were only missing between 7 and 17 minutes worth of data. Due to this limitation, each data set was used to generate strip charts that included only the data points.

A second limitation was that the data from each location (Malone, Florida, Middletown, California, and Kodiak, Alaska) covered no more than two days during the same time of the year. No comparison could be made to determine seasonal trends nor to verify that the data received was normal for each time of year. In order to perform a rigorous treatment of the data and to implement a controller, a significant amount of data would need to be collected during different seasons and under varying atmospheric conditions. Since this was not the case, additional testing on actual equipment under varying conditions is required prior to implementation of the proposed algorithm.

A third limitation was that the data sets included the effects of CALOC. Due to Loran-C's significant role in coastal navigation, there was no acceptable method to collect uncorrected data from an operational Loran-C chain; without CALOC's control input, the Loran-C chain would transmit an inaccurate signal during the time of data colletion. This required deriving a method for removing as much of CALOC's influence as possible so that the new contoller would have raw data that only included the inherent noise due to the propagation path, man-made interference, atmospheric noise, etc.

2.1.2 Data Preprocessing

There was little that could be done to mitigate the limitations of incomplete data sets and limited seasonal variation; however, it was believed that the effects of CALOC on the data set could be removed. The data sets, once plotted, revealed a significant delay between the time CALOC ordered an LPA and the time that its full effect was detected at the monitoring station. Thus, the first step in removing the effect of CALOC on the data was to determine the average time of this processing delay. After loading the data set, the preprocessing involves manually determining the timing of LPAs within the data set and then removing them using a time-phased correction described below.

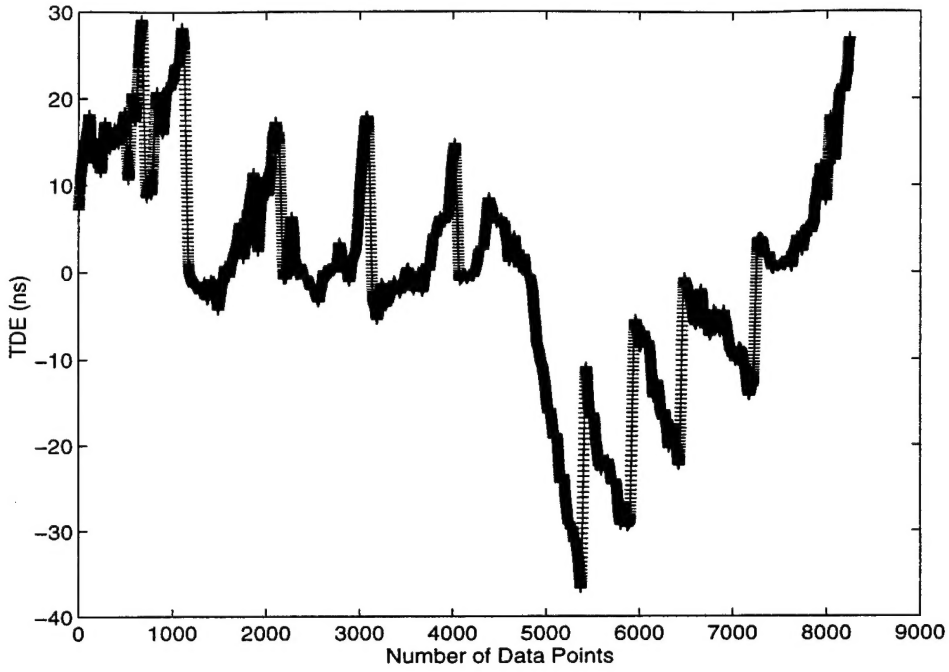

Figure 1: South-East United States Loran-C Station Yankee Time Difference Error recorded on 18 January 1997.

Based on the strip charts generated by CALOC that were provided with the data sets, it appeared that the time delay experienced between CALOC ordering a correction and its effect being detected at the monitor station was relatively constant. As a first order approximation, it was assumed that this delay was less than the 7.5 minute sampling interval presently used in CALOC. However, upon further investigation, it was found that the average time delay was on the order of 56 data points, or over nine minutes. Identification of the source of this time delay is beyond the scope of this work.

To determine the magnitude of the time delay, a moving average over 45 data points, equating to CALOC's 7.5 minutes average interval, was taken of each data set and plotted. The time delay was displayed in the graph by a vertical change in the time difference error (TDE) as may be seen in Figure 1. The time delay was determined by counting the number of 10-second samples between the indication in the data of an LPA and the indication that the pulse transmitter had shifted to the new transmission time.

Based on 146 LPAs in the nine data sets, the average time delay was computed to be 556.4 seconds. In order to apply the correction to remove the LPAs due to CALOC, the time delay was rounded up to 560 seconds, which equated to 56 10-second data points. The LPAs were then removed by applying the inverse of the LPA uniformly over the 56 data points. The same data described above, after removing the LPAs, may be seen in Figure 2. The time delay displayed no dependence on the magnitude of the ordered LPA since it was consistent for both a ± 20 ns LPA or a ± 40 ns LPA. This indicated that the delay was due solely to the time required to apply the LPA to the pulse transmitter.

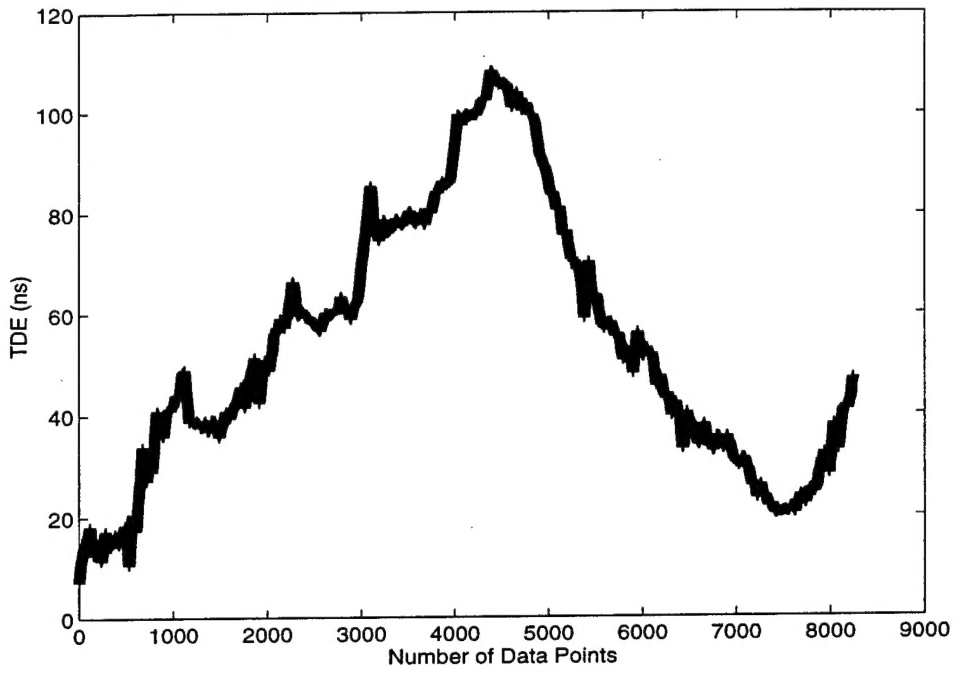

Figure 2: South-East United States Loran-C Station Yankee Time Difference Error recorded on 18 January 1997 with CALOC Local Phase Adjustments (LPAs) Removed.

2.2 Finite Impulse Response (FIR) Filter

The recorded Loran-C data contains high frequency noise components that need to be removed. These are due primarily to noise sources in the wireless medium, but also include noise from the transmitter and receiver. Additional noise is injected in the data during the preprocessing. To remove these high frequency noise sources, a digital low-pass filter is required. There are two basic types of digital filters: finite impulse response (FIR) and infinite impulse response (IIR). An FIR filter was selected primarily due to its linear phase characteristic. Other benefits of the FIR filter are that it is simpler to design and, when windowed, is of finite duration.

There are several methods of FIR filter design that may be used, including frequency sampling and windowing. The windowing method truncates an infinite duration unit sample response, $h_d(n)$, to length $M-1$ by multiplying $h_d(n)$ by a rectangular window of length M, defined as:

$$w(n) = \begin{cases} 1, & n = 0, 1, \ldots, M-1 \\ 0, & \text{otherwise.} \end{cases} \tag{1}$$

A symmetric lowpass linear-phase FIR filter is described in the frequency domain as:

$$H_d(\omega) = \begin{cases} e^{-j\omega\frac{(M-1)}{2}}, & 0 \leq |\omega| \leq \omega_c \\ 0, & \text{otherwise.} \end{cases} \tag{2}$$

A windowed FIR filter of length M has a unit sample response

$$h(n) = \frac{\sin \omega_c (n - \frac{M-1}{2})}{\pi (n - \frac{M-1}{2})}, \qquad 0 \leq n \leq M-1, n \neq \frac{M-1}{2} \tag{3}$$

where ω_c is the cut-off frequency and M is the filter length. Using a rectangular window has one significant drawback; it causes relatively large sidelobes. To eliminate the sidelobes, a window function that gradually decays toward zero is desirable. [4]

There are several windowing options available. Here we use the Hamming window, which is given as:

$$w(n) = 0.54 - 0.46 \cos(\frac{2\pi n}{M-1}), \qquad 0 \leq n \leq M-1 \tag{4}$$

where M is the window length or filter length. The Hamming window has significantly lower sidelobes compared to the rectangular window. However, for the same length filter, the width of the main lobe is wider which leads to a wider transition region in the FIR filter response. [4] The filter used in this application is an FIR filter with a Hamming window of length 32 and a cut-off frequency of $\pi/45$. The cut-off frequency was selected based on the removal of all high frequency components beyond the 45 data points used in each average.

The parameters needed to generate the FIR filter are the window length, M, and the cut-off frequency, ω_c; the outputs are the filter coefficients. The values used here are M = 32, and $\omega_c = \pi/45$. The response of the FIR filter using Hamming window is shown in Figure 3. It has a peak sidelobe level of approximately -45 dB while maintaining linear phase.

2.3 Proportional-Integral-Derivative (PID) Controller

The process began with exploring a model of the existing control system and implementing that model. Based on the model, suitable weights were derived for the controller, and then the algorithm was tested using all the data sets.

2.3.1 Theory

The PID controller is widely used in industrial processes to control systems that cannot be modeled as lumped and linear time-invariant. It is essentially three controllers in one: a proportional controller, an integral controller and a derivative controller. [5]

The transfer function of the proportional controller is a gain, k_p. For a given controller input, $e(t)$, the output will be:

$$u(t) = k_p e(t). \tag{5}$$

For a stable plant, the feedback system will remain stable for a range of k_p. However, as k_p increases, the unit-step response may become faster and the feedback system becomes unstable. One significant limitation to the proportional controller is that for the same

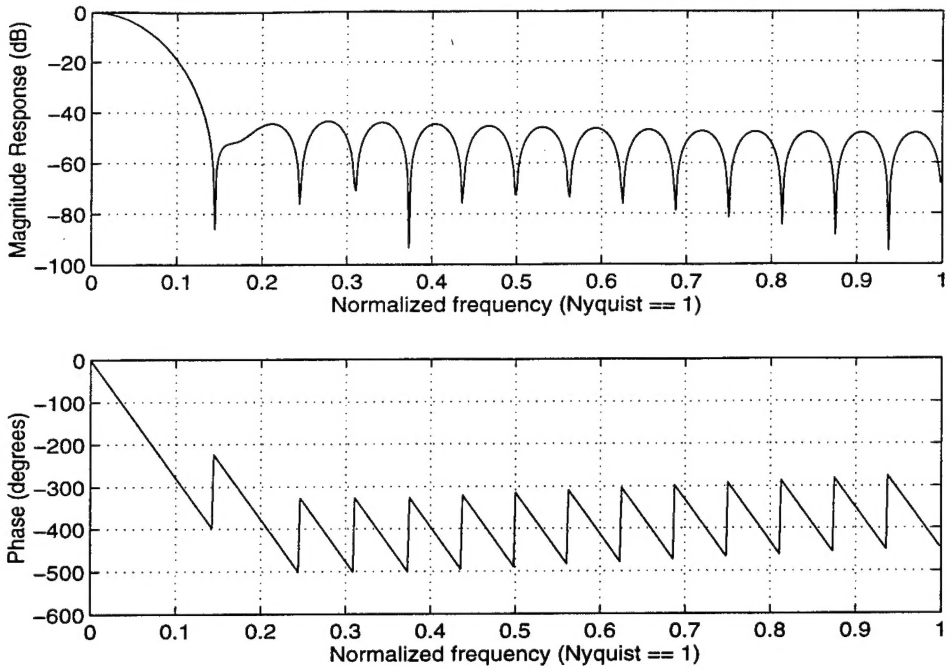

Figure 3: Magnitude and Phase Response for Finite Impulse Response (FIR) Filter (Length = 32, Cut-off Frequency = $\pi/45$) with Hamming Window.

unit-step reference input, the steady-state plant output will be different for different values of k_p requiring the plant set point to be manually reset. [5]

For the same input, the integral controller output is:

$$u(t) = k_i \int_0^t e(\tau) d\tau \tag{6}$$

where k_i is the integral constant. This leads to a transfer function for the integral controller of $\frac{k_i}{s}$. For a stable feedback system, the steady-state error due to any step-reference input is zero for all k_i. This means that there is no need to manually reset the set point when k_i is changed. For this reason, integral control is also called reset control with k_i being the reset rate. Though the requirement to reset the set point has been eliminated, the integral controller makes stabilizing the feedback system more difficult. [5]

The derivative controller maintains control of a system by using the rate of change of the error signal as its input. The output of the derivative controller is:

$$u(t) = k_d \frac{de(t)}{dt} \tag{7}$$

where $e(t)$ is the input to the controller and k_d is the derivative constant. The derivative controller by itself is rarely used in feedback control systems because if the error signal changes slowly or is constant, the controller output would be minimal or zero allowing a potentially large error to remain. [5]

A PID controller simultaneously takes advantage of all three controllers described above. The three parameters of the controller, k_p, k_i and k_d, are tuned to achieve the

desired system response. One method of tuning is by trial-and-error, initializing each parameter to some constant value and varying all three parameters to achieve a satisfactory system output. Exact values of these parameters could not be obtained due to lack of an accurate model for the entire Loran-C control subsystem. Because of this, a trial-and-error approach was used to obtain the solution described here. [5]

2.3.2 Model

The system model is a mathematical representation of the physical system. It may be used to evaluate the performance of the physical system to different input stimuli when the system is unavailable for operational testing, as is the case for the Loran-C system. The model developed for the existing control system, shown in Figure 4, contains four major modules, each modelled as separate transfer functions: CALOC, the transmitter, the medium and the monitoring station.

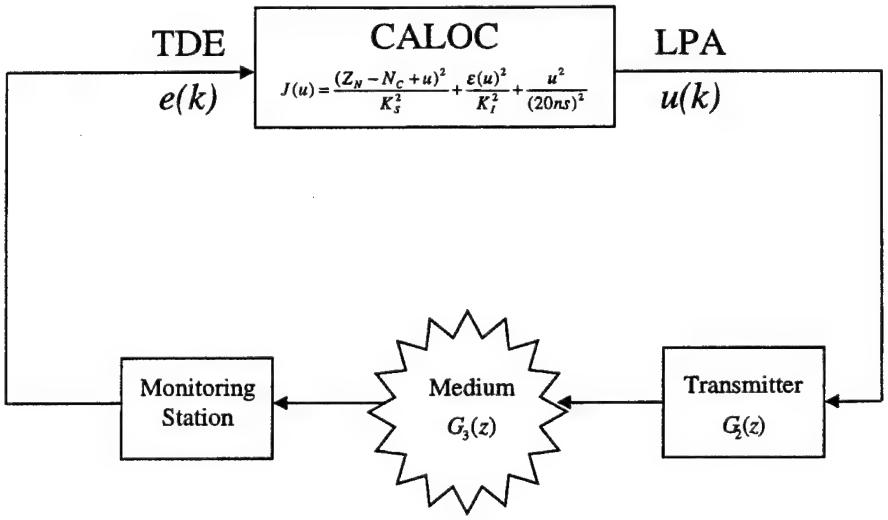

Figure 4: Loran-C Control System Model.

Knowledge of the transfer functions for the transmitter, medium and the monitoring station is not required based on the method of data preprocessing discussed earlier. The preprocessing only removed the effect of CALOC while leaving intact all noise components and the dynamic behavior of the transmitter, the medium, and the monitoring station equipment. Some modifications to the model were required to support simulation of the new control system. A method to input local phase adjustments (LPAs) in the data was developed to simulate the functionality of the new control algorithm within the Loran-C control system. As depicted in Figure 5, the simlation model sums the generated LPA with the future time difference errors (TDEs) from the recorded data. The LPA process was modelled as an integrator and time delay with a transfer function of:

$$G_L(z) = \frac{z}{z-1}z^{-1}. \tag{8}$$

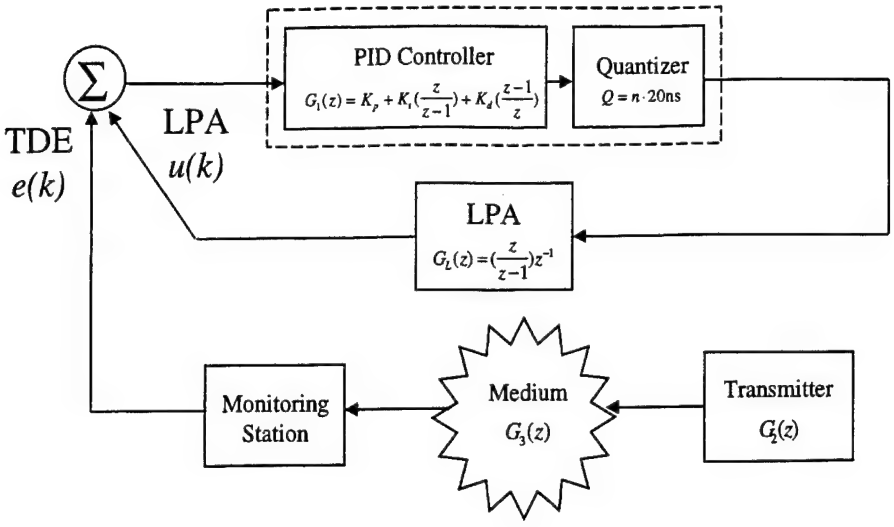

Figure 5: Simulation Model of the Loran-C Control System.

The LPA is a timing adjustment to the Loran-C station pulse transmitter for all future transmissions which leads to modelling the LPA function as an integrator. The single time delay was based on the fact that the effect of the LPA was detected at the monitoring station in about one 7.5-minute control interval.

The algorithm for the PID controller is the classical model shown in Figure 6. The input to the controller is the TDE at time k and the output is the continuous time LPA recommendation for time k. The proportional gain, K_p, is applied to the TDE directly. The integral of the TDE is the cumulative TDE and is controlled using the integral gain, K_i. The error rate of change is calculated by taking the difference between $e(k)$ and $e(k-1)$. The derivative gain, K_d, is applied to this difference. Summing all three contributions of the PID controller yields the LPA output that is then provided as input to the quantizer, which yields discretized values, $u(k)$.

Here, quantization is used to transform the LPA output of the controller into quanta of 20 ns, over a range of ± 180 ns, for use in controlling pulse transmission timing. The mid-tread quantizer is used as it did not introduce a bias to the signal [4]. The step size is a uniform value of 20 ns, which yields a maximum quantization error of 10 ns throughout the dynamic range of the quantizer. The quantization error for each sample may be modeled as a zero-mean, uniform random variable over the interval ± 10 ns.

2.4 PID Results

The PID control algorithm proved to be a definite improvement over the curve-fit algorithm in the existing Loran-C controller. In every case, both the current time difference error (TDE) and the cumulative TDE are maintained in closer control. In some cases, the PID controller was even able to accomplish this with fewer local phase adjustments (LPAs) than CALOC. However, in eight cases out of 29 there are a large number of LPAs

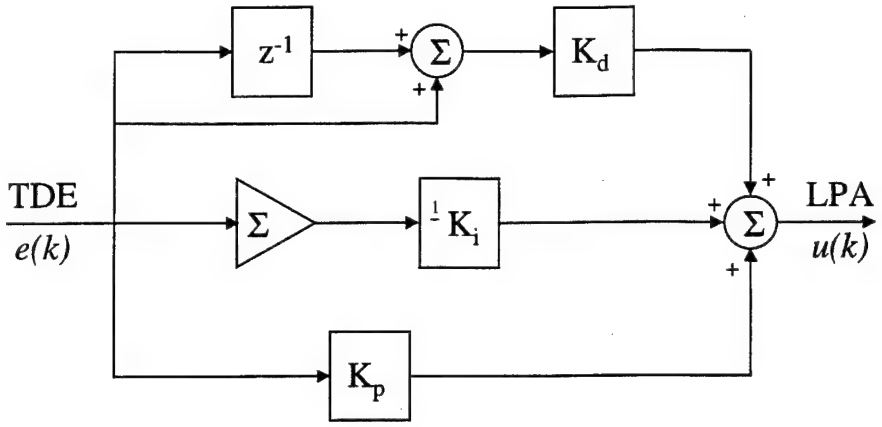

Figure 6: PID Controller without Quantization.

being ordered which is counter to one of the USCG control policies: to minimize the number of LPAs. This excessive chatter of the controller could be minimized with further operational testing using a greater number of data sets.

The results are presented for two Loran-C stations: SEUS Station Yankee and SEUS Station Zulu. SEUS Station Yankee cumulative TDE was initialized at -31 ns based on the actual value found on the CALOC strip chart. As is shown in Figure 7, CALOC maintained the current TDE within a range of -37 ns to 28 ns while the cumulative TDE has a range of ±50 ns. The PID controller showed a 14% improvement in dynamic range in both current TDE, with a range of -30 ns to 26 ns, and cumulative TDE, with a range of -40 ns to 46 ns.

The results for SEUS Station Zulu were even better. The cumulative TDE was initialized at -77 ns. As seen in Figure 8, CALOC was able to maintain the current TDE between -38 ns and 32 ns and the cumulative TDE between -71 ns and 38 ns. The PID controller was able to provide a significantly smaller dynamic range of cumulative TDE for Station Zulu. For the PID controller, the current TDE had a range of ±31 ns, an 11% improvement, and the cumulative TDE was maintained between -53 ns and 30 ns for a 24% improvement.

The results of the PID controller on the 29 data sets indicate that it is a viable option to CALOC. There was improved control of the TDE in every case though some data sets required a greater number of LPAs than the same data under CALOC. However, in the case of the data from the United States West Coast (USWC) Chain and the North Central United States (NOCUS) Chain, the chains are rarely in automatic control, which allows CALOC to function fully with no human intervention. Thus, the direct comparison with CALOC on those chains is not as conclusive.

Based on the overall results and the knowledge of the ever-changing medium in which Loran-C operates, the control algorithm needs to be data-dependent to better respond to this high noise environment. A PID controller could provide the needed adaptability; however, there are other controllers that are better suited.

3 Model Based Control Algorithm

Based on 146 LPAs in the nine data sets, the average time delay was computed to be 556.4 seconds. In order to apply the correction to remove the LPAs due to CALOC, the time delay was rounded up to 560 seconds, which equated to 56 10-second data points. The LPAs were then removed by applying the inverse of the LPA uniformly over the 56 data points. The same data described above, after removing the LPAs, may be seen in Figure 2. The time delay displayed no dependence on the magnitude of the ordered LPA since it was consistent for both a ± 20 ns LPA or a ± 40 ns LPA. This indicated that the delay was due solely to the time required to apply the LPA to the pulse transmitter.

3.1 Data-Dependent Solution

The primary reason for developing a data-dependent solution for the Loran-C control problem is the operating environment of the signal. The signal environment is a wireless media that is subject to these sources of interference, both natural and man-made. These sources of interference include atmospheric changes, terrain and electromagnetic intereference.

3.1.1 Atmospheric Effects

The sources of atmospheric effect on the Loran-C signal are primarily due to temperature changes and seasonal weather effects. The effect of temperature changes on signal propagation has no reasonable theoretical explanation other than its effect on the refractive index of the media. Specifically, the Loran-C signal exhibits a diurnal variation that can be associated with temperature changes. [6] One source of these temperature effects is a temperature inversion and associated humidity change which may produce highly variable refractivity profiles. This process produces an evaporation duct in which radio waves may propagate well beyond the horizon. Overland propagation refraction effects may be seen in at least two situations: one is the evaporation of water on the ground after raining which produces an over-land evaporation duct, and the second is the radiational cooling over deserts and snow-covered terrain on clear nights which yields anomalous propagation. [7]

The seasonal weather effects on the Loran-C signal are caused by the passage of cold and warm fronts predominate at specific times of the year. The interpretation of the correlation between the time difference and total refractivity is that the passage of cold and warm fronts produce transient decreases in the propagation time delay. The cold front decreases occur after the front has passed while the decreases associated with the warm front occur before frontal passage. [6]

The conclusion that may be drawn from these effects is that the Loran-C signal is being influenced by changes in the refractive index well above the earth's surface. A more complete understanding of these atmospheric effects is required in order to make predictions. In the case of the Loran-C system, accurate predictions correspond directly with greater position accuracies. [6]

3.1.2 Terrain

The signal effects of terrain on the Loran-C signal are due to diffraction phenomena, which are exhibited in both diffuse scattering and coherent scattering. These phenomena may be broken down into two categories. The first is specific irregularities in the terrain, such as mountain ridges, which are often modeled as knife-edges or, in some cases, cylinders. Secondly, diffraction is produced by the curvature of the smooth spherical surface of the earth which applies to propagation over the ocean or in the plains. At low frequencies, diffraction by hills or ridges alters the field strength in a significant region around the line of sight which means that more than one diffracting feature on the terrain may be contributing to the propagation losses. This is a challenging issue that has not yet been successfully modeled for long ray-paths over varying terrains. [7]

3.1.3 Electromagnetic Interference

The sources for electromagnetic interference for the Loran-C system are essentially of two types: fixed radiators and mobile, or random, radiators. The fixed radiators are those that continuously transmit at a constant frequency or transmit at consistent times of the day while the mobile radiators randomly transmit their signal and maintain no pattern to their transmission. Each master-secondary baseline will have a different set of known radiators that may be relatively easily modeled. However, determining a suitable model for the mobile radiator may be quite involved and location dependent.

Two fixed radiators that are significant contributors to electromagnetic interference are overhead power lines and radio towers. The power lines are low power signals that exist within the Loran-C frequency band. This has become of particular interest since the expansion of the Loran-C system across the North American continent. The signal amplitudes vary as a function of the square of the distance from the power line, so their effect is only critical near to the power line, on the order of one mile. However, because so many power lines exist, using notch filtering to remove the effects is not feasible. Radio towers along the ray-path also contribute to the electromagnetic interference seen by the Loran-C signal. One example of this is the frequency shift keying found at naval communications stations. These, however, unlike the power lines, may be divided using superposition and treated as either deterministic or random noise when considering their effects on the time of arrival. [8]

One example of the mobile, or random, radiator that causes electromagnetic interference with the Loran-C signal is the cathode ray tube (CRT). The raster scan displays on computers and test instruments cause interference due to the harmonics of the horizontal scan frequency. These frequencies are extremely stable and may be isolated once the device is identified. [8] There are other sources of random electromagnetic interference that would also need to be accounted for. One prominent example is the ham radio operator that may be infrequently transmitting near the operating frequency of Loran-C. The mobile radiator presents a unique challenge in that their signal, in the aggregate, is a non-deterministic, random process.

3.2 Kalman Filter

Kalman filtering provides several advantages over the PID algorithm in solving the Loran-C control problem. Its mathematical formulation is described in state-space form, and its solution is computed recursively. Thus, each updated state estimate is computed only from the previous estimate and the new input data which requires only that the previous state estimate be stored. The Kalman filter is also more efficient than computing the next state estimate using the entire past observed data at each step in the process. [9]

3.2.1 Model

In the general case, the Kalman filtering problem is stated in terms of two vectors of random variables: an M-dimensional parameter $\mathbf{x}(k)$ which denotes the state of a discrete-time, linear, dynamic system and $\mathbf{y}(k)$ which denotes the observed data of the system. The system model may then be fully described by two equations: a process equation and a measurement equation. [9]

The process equation is:

$$\mathbf{x}(k+1) = \mathbf{A} \cdot \mathbf{x}(k) + \mathbf{v}(k) \tag{9}$$

where $\mathbf{A}$ is an $M \times M$ state transition matrix that relates the system state at times k and $k+1$. The $M \times 1$ vector $\mathbf{v}(k)$ represents process noise and is modeled as a zero-mean, white-noise process, ideally Gaussian. [9]

The measurement equation, which describes the observation vector, is:

$$\mathbf{z}(k) = \mathbf{C} \cdot \mathbf{x}(k) + \mathbf{\Delta w}(k) \tag{10}$$

where $\mathbf{C}$ is an $N \times M$ measurement matrix. The $N \times 1$ vector $\mathbf{\Delta w}(k)$ represents measurement, or sensor, noise and is modeled as another zero-mean, white-noise process, ideally Gaussian. [9]

The Kalman filter attempts to use the past observed data values, consisting of $\mathbf{y}(0)$, ..., $\mathbf{y}(k)$, and the model to predict the minimum mean-square estimate of the new state, $\mathbf{x}(k+1)$. Thus, the Kalman filter is attempting to solve the equation:

$$\mathbf{x}(k+1) = \mathbf{A} \cdot \mathbf{x}(k) + \mathbf{L}(k) \cdot [\mathbf{z}(k) - \mathbf{C} \cdot \mathbf{x}(k)] \tag{11}$$

where $\mathbf{z}(k)$ - $\mathbf{C} \cdot \mathbf{x}(k)$ is the correction to be applied and $\mathbf{L}(k)$ is determined in order to minimize $\Sigma \parallel \tilde{\mathbf{x}}(k) \parallel^2$ where the error, $\tilde{\mathbf{x}}(k) = \mathbf{x}(k)$ - $\hat{\mathbf{x}}(k)$.

In tailoring the general model to the specific case of the Loran-C control problem, depicted in Figure 9, several adaptations were made. In Equation 9, the first term becomes $\mathbf{x}(k) + \Delta\Phi(k)$ yielding a new process equation of

$$\mathbf{x}(k+1) = \mathbf{x}(k) + \Delta\Phi(k) + \mathbf{v}(k) \tag{12}$$

where x(k) is the estimate of the current TDE and $\Delta\Phi(k)$ is the input LPA. Similarly, the first term in Equation 10 becomes $\mathbf{z}(k) + \mathbf{x}(k)$ yielding a new measurement equation of

$$\mathbf{z}(k+1) = \mathbf{z}(k) + \mathbf{x}(k) + \mathbf{\Delta w}(k) \tag{13}$$

where $\mathbf{z}(k)$ is the cumulative TDE.

The long-term fluctuations of 12-24 hours were of lesser consequence since the control of the time difference (TD) would be over a much shorter period. A suitable model for the short-term fluctuations in the time difference error (TDE) is a random walk with additive white Gaussian noise as depicted in Figure 10. The model is characterized by the equation:

$$\mathbf{w}(k) = \mathbf{w_m}(k) + \mathbf{\Delta w}(k) \tag{14}$$

where

$$\mathbf{w_m}(k) = \mathbf{w_m}(k-1) + \mathbf{v}(k-1) \tag{15}$$

with $\mathbf{w}(k)$ and $\mathbf{v}(k)$ being zero mean, uncorrelated, white Gaussian noise.

3.2.2 Optimal Controller

Based on the model described above, the Kalman filter estimates the whole state as defined by:

$$\hat{\mathbf{x}}(k+1) = \hat{\mathbf{x}}(k) + \mathbf{\Delta\Phi}(k) + \frac{\mathbf{p}(k)}{\mathbf{R}+\mathbf{p}(k)}(\mathbf{\Phi_e}(k) - \hat{\mathbf{x}}(k)) \tag{16}$$

$$\mathbf{p}(k+1) = \mathbf{p}(k) + \mathbf{Q} - \frac{\mathbf{p}(k)^2}{\mathbf{R}+\mathbf{p}(k)} \tag{17}$$

$$\hat{\mathbf{z}}(k+1) = \hat{\mathbf{z}}(k) + \hat{\mathbf{x}}(k) \tag{18}$$

where $\hat{\mathbf{x}}(k)$ is the TDE estimate, and $\hat{\mathbf{z}}(k)$ is the estimate of the cumulative TDE. The constants $\mathbf{Q}$ and $\mathbf{R}$ are defined as

$$\mathbf{Q} = \mathrm{cov}(\mathbf{v}(k)) \tag{19}$$

$$\mathbf{R} = \mathrm{cov}(\mathbf{\Delta w}(k)). \tag{20}$$

In order to devise an optimal controller, a control law must be defined. As discussed in the previous section, the USCG has established Loran-C control procedures concerning the allowed range of time difference and minimizing the number of LPAs. The metric that is used to measure the performance of the controller is a cost function, defined as:

$$\mathbf{J}(k) = \sum_{k=0}^{\infty} \{\sigma_1 |\hat{\mathbf{x}}(k)|^2 + \sigma_2 |\hat{\mathbf{z}}(k)|^2 + |\mathbf{\Delta\Phi}(k)|^2\} \tag{21}$$

where $\hat{\mathbf{x}}(k)$ is the estimate of the current TDE, $\hat{\mathbf{z}}(k)$ is the estimate of the cumulative TDE, and $\mathbf{\Delta\Phi}(k)$ is the LPA. The cost function is similar to the one defined for CALOC in that it applies a cost to a large TDE, a large cumulative TDE, and a large LPA. Control of the process is defined by

$$\Delta\Phi(k) = -\mathbf{L}(k) \begin{bmatrix} \hat{\mathbf{x}}(k) \\ \hat{\mathbf{z}}(k) \end{bmatrix} \tag{22}$$

where $\mathbf{L}(k)$ is determined recursively using the Matlab function *dlqr*, which solves the discrete-time linear-quadratic regulator problem and the associated Riccati equations.

3.3 Results

As in the case of the PID controller, the Kalman filter improved the control of the time difference error (TDE) over the existing Loran-C controller. It was also an improvement over the PID controller and, in most cases, inserted fewer local phase adjustments (LPAs). The results detailed below compare the PID control algorithm to the Kalman filter as the PID has already been shown to be superior to the existing controller. The same two Loran-C stations used in the preceeding section are used here to illustrate the improvement of the Kalman filter.

The initial cumulative TDE values for SEUS Stations Yankee and Zulu are the same as for the PID controller: -31 ns and -77 ns, respectively. As may be seen in Figure 11, the Kalman filter essentially maintained the same range for current TDE while improving control of the cumulative TDE. The range for the current TDE for the Kalman filter was -30 ns to 29 ns as compared to a range of -30 ns to 26 ns for the PID controller. However, the Kalman filter showed a 31% improvement in cumulative TDE with a range of -26 ns to 33 ns compared to the PID controller with a range of -40 ns to 46 ns.

The improvement of the results for SEUS Station Zulu were more pronounced. Similar to Station Yankee, Station Zulu maintained the current TDE within a similar range: -31 ns to 36 ns as compared to $\pm$31 ns for the PID controller. As Figure 12 illustrates, the range of cumulative TDE for the Kalman filter was -33 ns to 32 ns as compared to -53 ns to 30 ns for the PID controller, a 34% improvement.

4 Conclusions and Recommendations

In this work, two control algorithms have been designed and tested on the available data: a classical PID controller and a model based Kalman filter/optimal control.

The PID control algorithm blends the strengths of three controllers into one: a proportional controller, an integral controller, and a derivative controller. This algorithm was developed using a basic model and tuned using a trial-and-error approach to provide the best control. The results indicate that this algorithm provides more accurate pulse transmission timing than CALOC.

The Kalman filter was explored as an alternative to the PID controller. The filter provides the capacity to be adaptive in a changing environment and is much more robust than the PID controller. This is an extremely important part of what is needed in the future control system for Loran-C in today's technological environment. The preliminary results of the Kalman filter showed an even greater improvement over the existing controller than the PID controller.

Further study of the Loran-C control system will be valuable in at least three areas. First, an accurate mathematical model of the Loran-C control system needs to be developed. This will provide the opportunity to easily evaluate possible improvements to Loran-C while minimizing the operational testing required under normal situations. Second, the PID controller needs to be fully operationally tested to determine what further tuning is required prior to implementation. This will provide a suitable bridge between what exists today and the controller of the future. The PID controller will remove the necessity for the Loran-C station operators to second-guess the system. Finally, the Kalman filter needs to be developed further in order to become fully operational.

References

[1] Frederick M. France, Jr., "Design of an Algorithm for Minimizing LORAN-C Time Difference Error," Electrical Engineer Degree Thesis, Naval Postgraduate School, Monterey, CA, September 1997.

[2] "Project W1234, Consolidated Control," United States Coast Guard, Electronics Engineering Center, Wildwood, NJ, June, 1995.

[3] D. Feldman, "On the Modeling, Estimation and Control of LORAN-C Time Differences," United States Coast Guard, Electronics Engineering Center, Wildwood, NJ, February, 1975.

[4] John G. Proakis and Dimitris G. Manolakis, *Digital Signal Processing: Principles, Algorithms, and Applications*, MacMillan Publishing Company, NY, 1993.

[5] Chi-Tsong Chen, *Analog and Digital Control System Design: Transfer-Function, State-Space, and Algebraic Methods*, Saunders College Publishing, NY, 1992.

[6] Robert H. Doherty and J. Ralph Johler, "Meteorological Influences on Loran-C Ground Wave Propagation," United States Department of Commerce, Office of Telecommunications, Institute for Telecommuncations, Boulder, CO, September, 1973.

[7] M. L. Meeks, *Radar Propagation at Low Altitudes*, Artech House, Inc., Dedham, MA, 1982.

[8] B. B. Peterson and R. J. Hartnett, "Measurement Techniques for Narrowband Interference to LORAN," Center for Advanced Studies, United States Coast Guard Academy, New London, CT, October, 1990.

[9] Simon Haykin, *Adaptive Filter Theory*, Prentice Hall, Inc., Englewood Cliffs, NJ, 2nd Edition, 1991.

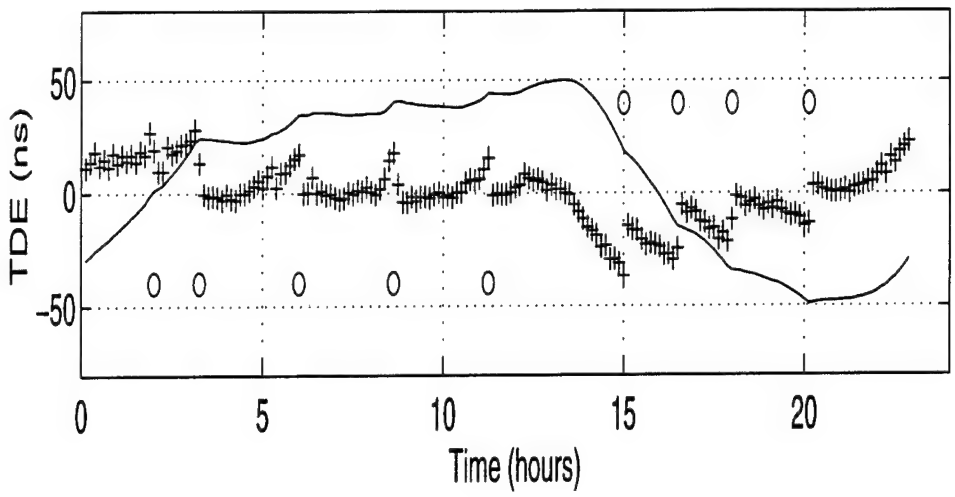

(a) CALOC

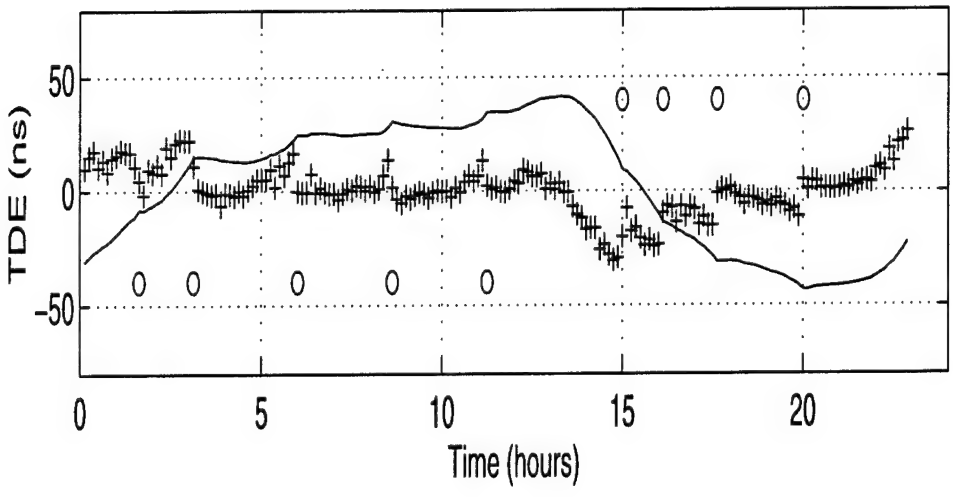

(b) PID Controller

Figure 7: Strip Chart for South East United States (SEUS) Loran-C Chain Station Yankee recorded on 18 January 1997: **o** Linear Phase Adjustment (LPA) (magnitude times 2); + Time Difference Error (TDE); — Cumulative TDE.

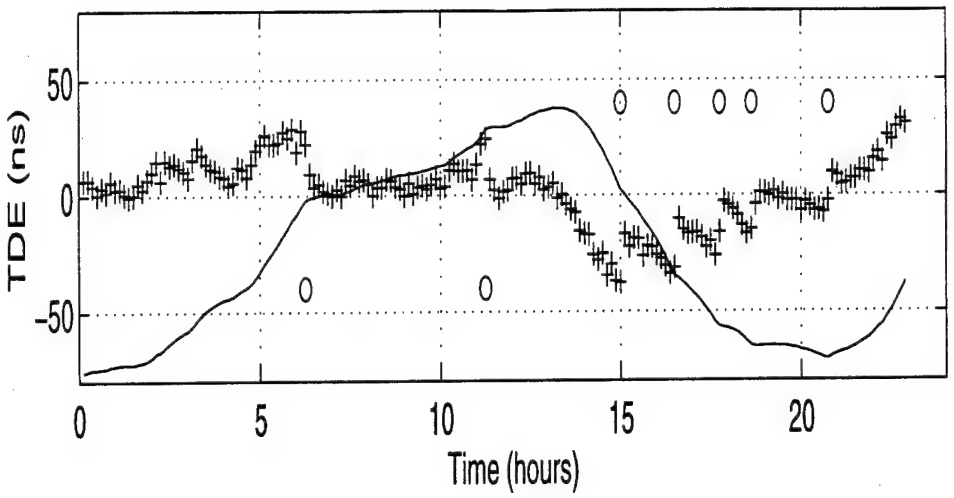

(a) CALOC

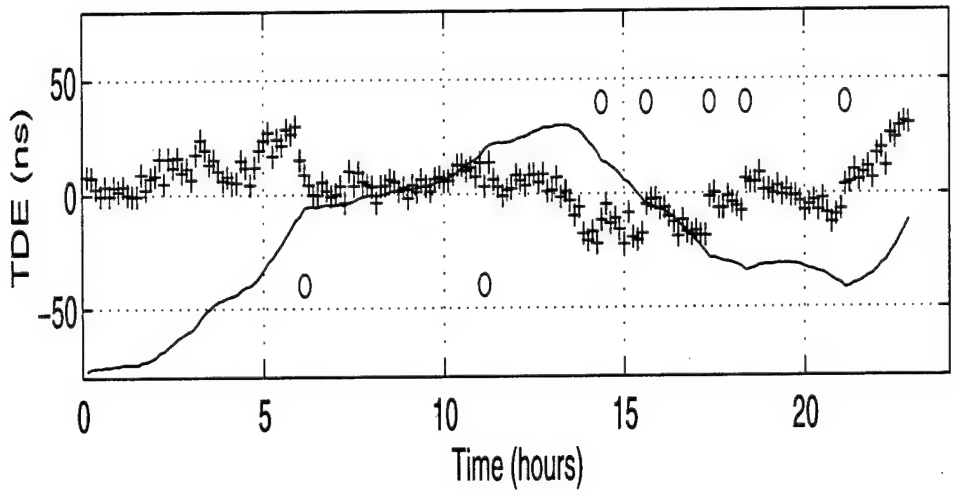

(b) PID Controller

Figure 8: Strip Chart for South East United States (SEUS) Loran-C Chain Station Zulu recorded on 18 January 1997: o Linear Phase Adjustment (LPA) (magnitude times 2); + Time Difference Error (TDE); — Cumulative TDE.

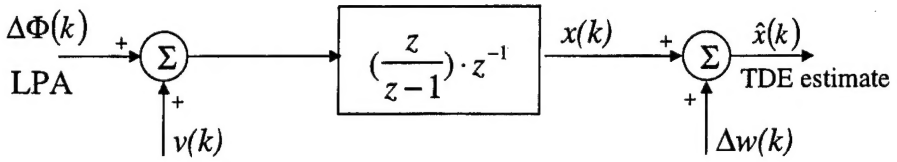

Figure 9: Control System Process Model.

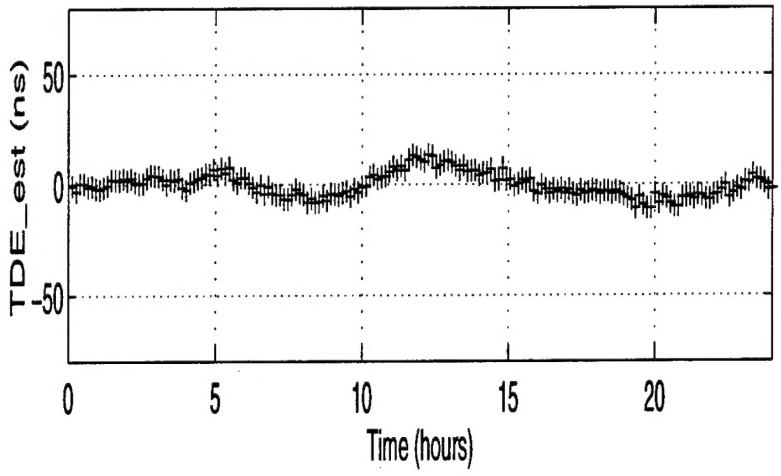

Figure 10: Random Walk with Additive White Gaussian Noise

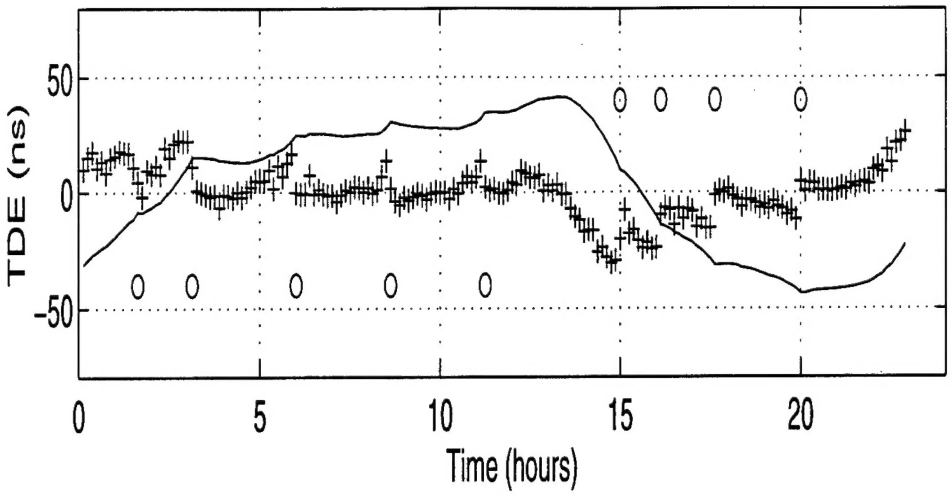

(a) PID Controller

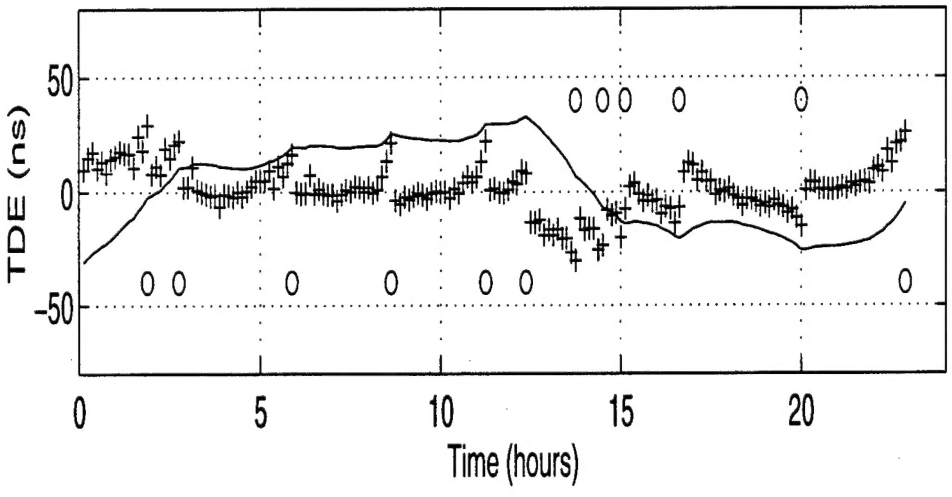

(b) Kalman Filter

Figure 11: Strip Chart for South East United States (SEUS) Loran-C Chain Station Yankee recorded on 18 January 1997: o Linear Phase Adjustment (LPA) (magnitude times 2); + Time Difference Error (TDE); — Cumulative TDE.

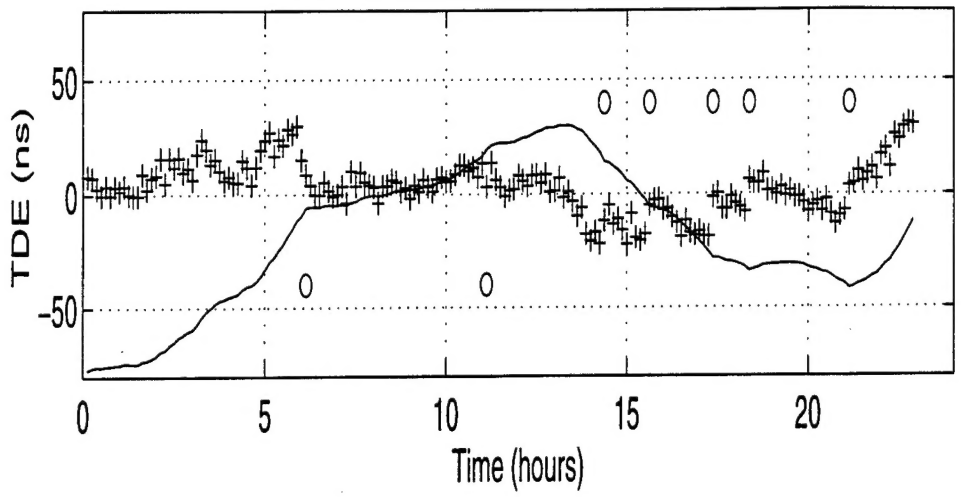

(a) PID Controller

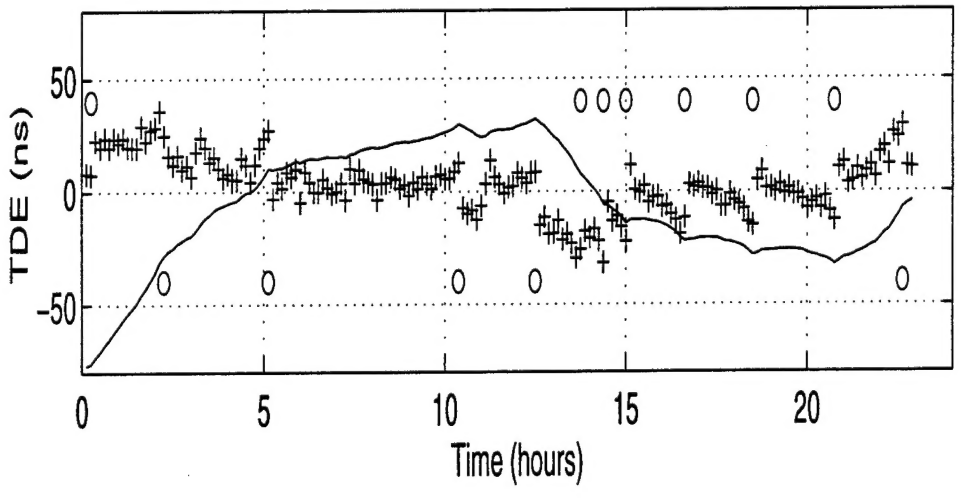

(b) Kalman Filter

Figure 12: Strip Chart for South East United States (SEUS) Loran-C Chain Station Zulu recorded on 18 January 1997: o Linear Phase Adjustment (LPA) (magnitude times 2); + Time Difference Error (TDE); — Cumulative TDE.

Distribution List

- Defense Technical Information Center 2
  8725 John J. Kingman Rd., Ste 0944
  Ft. Belvoir, VA 22060-6218

- Dudley Knox Library 2
  Naval Postgraduate School
  411 Dyer Rd.
  Monterey, CA 93943-5101

- Research Office, Code 09 1
  Naval Postgraduate School
  589 Dyer Road
  Monterey, CA 93943-5138

- Chairman, Code EC 1
  Department of Electrical and Computer Engineering
  Naval Postgraduate School
  Monterey, CA 93943-5121

- Prof. Murali Tummala, Code EC/Tu 4
  Department of Electrical and Computer Engineering
  Naval Postgraduate School
  Monterey, CA 93943-5121

- Prof. Roberto Cristi, Code EC/Cx 1
  Department of Electrical and Computer Engineering
  Naval Postgraduate School
  Monterey, CA 93943-5121

- Commanding Officer 1
  U.S. Coast Guard
  Loran Support Unit
  12001 Pacific Avenue
  Wildwood, NJ 08260-3232

- LT Steve Bartlett 2
  U.S. Coast Guard
  Loran Support Unit
  12001 Pacific Avenue
  Wildwood, NJ 08260-3232

- LT Frederick M. France, Jr., USN 1
  1048 Spruance Road
  Monterey, CA 93940-4821